IOP Publishing Superconductor Science and Technology
Supercond. Sci. Technol. 31 (2018) 015006 (7pp) https://doi.org/10.1088/1361-6668/aa96f5

Effect of cooldown and residual magnetic field on the performance of niobium–copper clad superconducting radio-frequency cavity

Pashupati Dhakal and Gianluigi Ciovati

Jefferson Lab, Newport News, VA 23606, United States of America

E-mail: dhakal@jlab.org

Received 4 May 2017, revised 27 October 2017
Accepted for publication 30 October 2017
Published 22 November 2017

Abstract

We present the results of rf measurements on a niobium–copper clad superconducting radio-frequency cavity with different cooldown conditions and residual magnetic field in a vertical test Dewar in order to explore the effect of thermal current induced magnetic field and its trapping on the performance of the cavity. The residual resistance, extracted from the $Q_0(T)$ curves in the temperature range 4.3–1.5 K, showed no dependence on a temperature gradient along the cavity during the cooldown across the critical temperature up to $\sim$50 K m^{-1}. The rf losses due to the trapping of residual magnetic field during the cavity cooldown were found to be $\sim$4.3 nΩ μT^{-1}, comparable to the values measured in bulk niobium cavities. An increase of residual resistance following multiple cavity quenches was observed along with evidence of trapping of magnetic flux generated by thermoelectric currents.

Keywords: niobium, superconducting cavities, flux expulsion, NbCu

(Some figures may appear in colour only in the online journal)

1. Introduction

Superconducting bulk niobium has been the material of choice for superconducting radio-frequency (SRF) cavities used in particle accelerators due to its highest superconducting transition temperature and highest lower critical field among the elemental superconductors. In addition, the niobium material is easier to fabricate into the complex shapes and sizes of SRF cavities. Significant amount of research work in SRF communities have been dedicated in order to explore the material alternative to the bulk niobium which can perform better and can be produced in more cost effective ways [1]. For examples, niobium thin film on copper [2] and higher transition temperature superconductors such as NbTiN [3], NbN [4], Nb_3Sn [5–7], MgB_2 [8] and multilayers [9]. Among these alternative materials, the niobium thin films on copper cavities have been explored widely. The advantage of thin niobium film on copper substrate is twofold; first the penetration of the rf field in SRF cavities is within first $\sim$50 nm which dictate the performance of SRF cavities and second; the higher thermal conductivity of Cu provides better thermal stability against thermal quench. Moreover, the lower material cost of Cu materials compared to high purity Nb can be advantageous for the SRF operating at lower frequencies since the surface area of the cavities are inversely proportional to the resonant frequency. It was also found that the Nb thin film cavities sputtered on Cu tend to have higher quality factors due to lower Bardeen–Cooper–Schrieffer (BCS) surface resistance and lower sensitivity to the residual earth magnetic field [2].

Alternative to the thin film of Nb deposited on the Cu cavities, the fabrication of bimetallic Nb/Cu cavities were explored [10–12] for the same reasons of reduced material cost and better thermal stability against the quench. The single cell cavities that were fabricated by hydroforming of Nb/Cu tubes showed accelerating gradients as high as 40 MV m^{-1}, comparable to the best bulk niobium cavities with much reduced Q-slope compared to the Nb thin film on Cu cavities. It is believed that the cooldown of these bimetallic cavities needed extra care due to the frozen magnetic flux generated due to the thermal current (Seebeck effect). The impact of the cooldown procedure on the magnetic flux trapping, the

Q-degradation after the cavity quench as well as the effect of thermal resistance of the Nb/Cu interface are still being investigated in several laboratories. In this manuscript, we present the result of rf measurements of a Nb/Cu clad cavity in order to explore the effect and the origin of residual magnetic flux trapping during the cavity cooldown and its impact on the rf performance of the cavity.

2. Experimental setup

The cavity labeled 1NC2 is a TESLA shaped cavity manufactured at DESY from a Nb/Cu clad tube by extrusion as a seamless unit. The thickness of the niobium layer was ~0.5 mm and the copper structure has a thickness of ~2.5 mm. Niobium beam tubes were electron beam welded on the seamless cavity. The detail of the cavity fabrication was presented in [11]. Prior to the tests reported in this article, the cavity was processed with buffer chemical polishing (BCP), high temperature annealing (800 °C/3 h), low temperature baking (145 °C/36 h) and rf tested several times [13]. During those tests, the cavity reached ~40 MV m^{-1} with quality factor of ~10^{10} at 2 K. The average final thickness of the Nb on Cu was approximately 0.3 mm after ~0.2 mm was removed via BCP.

During this study, standard procedures of high pressure rinse with ultra-pure water, drying in the ISO4/5 cleanroom, assembly of flanges with rf feedthroughs and pump out ports were applied before inserting the vertical test Dewar. Four Cernox temperature sensors were mounted at the irises and equator of the cavity to measure the cooldown rate. The distance between temperature sensors at top and bottom iris is ~19 cm. To measure the residual magnetic flux density at the cavity surface during the cooldown process, two Bartington single-axis flux-gate magnetometers were mounted on the cavity surface, directed along the cavity axis. One magnetic sensor was placed on the equator of the cavity; whereas the other sensor was placed on the beam tube to ensure the uniformity of the magnetic flux before the cooldown. The magnetic field uniformity within the cavity volume is ~ ±0.2 μT. Figure 1 shows the cavity, sensors and Helmholtz coil setup in vertical test stand.

The cavity cooldown process is as follows: (i) the magnetic field was set ~0.2 μT using the compensation coil in the Dewar and the cavity was cooled with the standard cooldown procedure at Jefferson Lab resulting in ~4 K temperature difference between the top and bottom iris. (ii) The temperature and magnetic field were recorded until the vertical Dewar is full with liquid He and a uniform temperature of ~4.3 K is achieved. (iii) Measurement of $Q_0(T)$ at low rf field (B_p ~ 10 mT) from 4.3 to 1.5 K was done using the standard phase-lock technique. (iv) The cavity was warmed-up above the critical temperature ($T_c \cong 9.25$ K) and cooled down to 4.3 K while keeping the temperature difference between two irises below 0.1 K. (v) $Q_0(T)$ was measured once more from 4.3 to 1.5 K. (vi) The current on the Dewar compensation coils was set at a different value, resulting in a different residual dc magnetic field and steps (ii)–(v) were repeated (the Helmholtz coil was not installed for this series of tests). Figure 2 shows the temperature and residual magnetic field at the cavity, B_a, during different cooldown regimes: 'fast' (temperature difference iris–iris ~4 K) and (b) 'slow' (temperature difference iris–iris <0.1 K) when the equator of the cavity reaches the critical temperature. Whereas a stable residual magnetic field is observed above T_c during a more uniform cooling, variations in the amplitude of the magnetic field at the cavity of up to ~0.3 μT were measured between 16 and 9.25 K in the presence of larger temperature gradients across the cavity. Such variations in magnetic field are related to thermoelectric currents flowing between the Nb and Cu layers as a result of the Seeback effect.

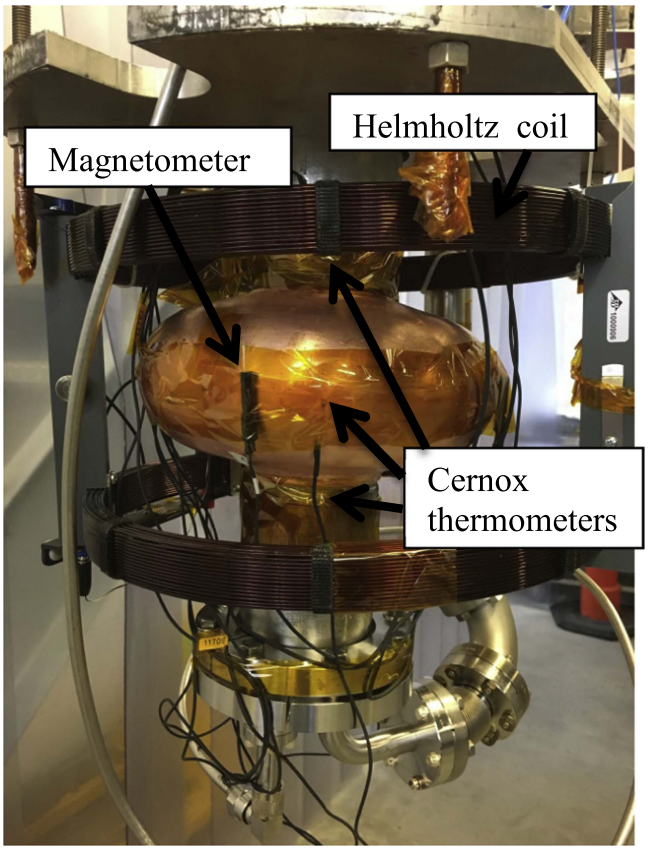

Figure 1. The schematic of the Nb/Cu clad cavity showing the magnetometer and temperature sensor locations.

3. Experimental results

The average rf surface resistance $R_s(T)$, shown in figure 3, was calculated from the $Q_0(T)$ data measured at low rf field (B_p ~ 10 mT) as $R_s(T) = G/Q_0(T)$, where $G = 271.65\ \Omega$ is the cavity geometry factor. The experimental $R_s(T)$ was fitted with the following equation

$$R_s(T) = R_{BCS}\left(T, \frac{\Delta}{k_B T_c}, l\right) + R_{res}, \quad (1)$$

where R_{res} is the temperature independent residual resistance and R_{BCS} is BCS surface resistance. Here, Δ is the superconducting energy gap at 0 K, k_B is Boltzmann's constant and

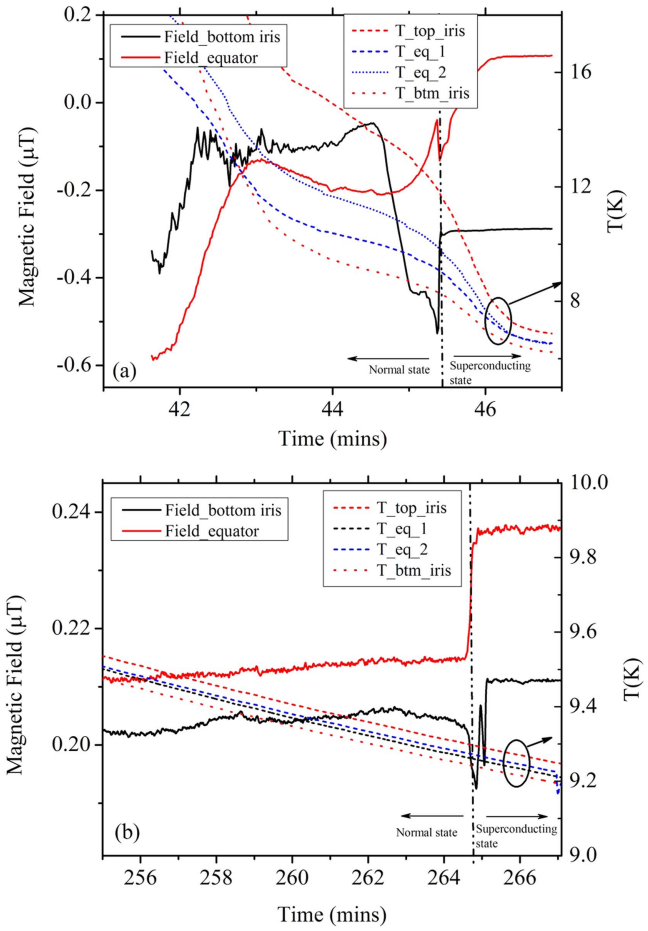

Figure 2. Temperature and residual dc magnetic field measured at the cavity during (a) 'fast' cooldown (Test #1) and (b) 'slow' cooldown (Test #2).

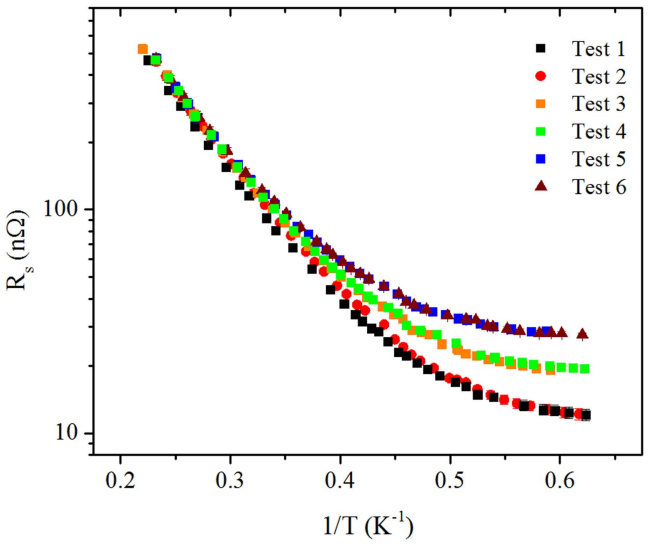

Figure 3. R_s versus $1/T$ after different cooldown cycles measured at low rf field ($B_p \sim 10$ mT). The test pairs (1, 2), (3, 4) and (5, 6) represent fast ($\Delta T/\Delta z \sim 22$ K m^{-1}) and slow ($\Delta T/\Delta z < 0.5$ K m^{-1}) cool-downs in different residual magnetic field. Please refer to table 1 for details about the residual field and temperature gradient during cooldown for each test.

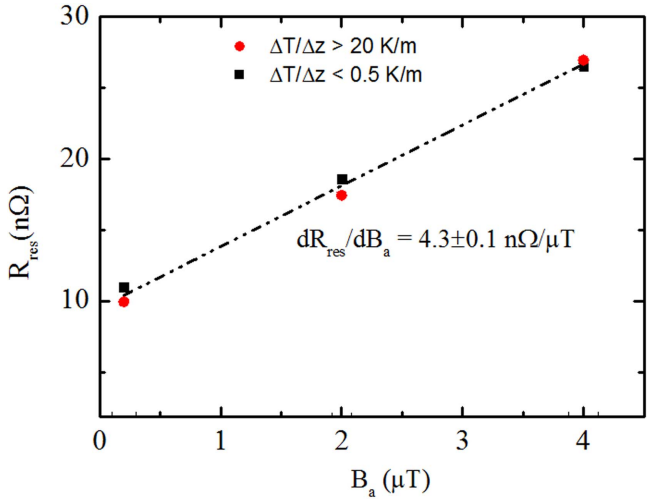

Figure 4. Residual resistance as a function of the residual magnetic field at the cavity for different temperature gradients at T_c. The residual field is the average of the values at the iris and equator at ~10 K, just before the cavity transition to the superconducting state.

l is the normal-electrons' mean free path. The BCS resistance was numerically calculated from the BCS theory of superconductivity, valid at low rf field [14] with parameters $T_c = 9.25$ K, London penetration depth ($\lambda_L = 32$ nm) and BCS coherence length ($\xi_0 = 39$ nm), considered to be material constants for superconducting niobium. Table 1 lists the values of R_{res} and $\Delta/k_B T_c$ extracted by fitting the data with equation (1) along with the residual field at the cavity just above T_c (average of the values at the equator and iris), the vertical temperature gradient $\Delta T/\Delta z$, the cooling rate $\Delta T/\Delta t$ at T_c and the ratio of the magnetic field just below T_c divided by the value just above T_c (B_{sc}/B_n) at the equator.

Figure 4 shows a plot of the residual resistance as a function of the residual magnetic field at the cavity location, just above T_c, showing no significant difference between 'fast' and 'slow' cooldown. As shown in figure 2(a), variations in the residual magnetic field during fast cooldown are sufficiently small that it would add less than 1 nΩ to the residual resistance.

Figure 5 shows the $Q_0(E_{acc})$ results at 2 K after each cooldown. The typical experimental error in Q_0 and E_{acc} is ~10% and ~5% respectively. The cavity was limited by quench at ~19 MV m^{-1}. The same cavity reached as high as ~40 MV m^{-1} during earlier rf test cycles. The cause of low field quench compared to previous tests is unknown. The cavity was stored in a cabinet for an extended period of time (~12 years), and contamination from foreign materials which might have landed on the inner surface could be a possible explanation for the degradation of the quench field. A Q-degradation of up to 10% was observed after a single quench. This phenomenon was reported in earlier tests of Nb/Cu clad cavities and it was attributed to additional magnetic flux generated by thermo-currents being created during the cavity quench. Further increase in residual resistance was observed when the cavity is subjected to several additional quenches. In earlier measurements, the increase in surface resistance was as high as ~10 nΩ with multiple quench events

Table 1. The residual resistance and superconducting gap extracted from the fit of equation (1) along with cooldown parameters and residual magnetic field. The cooling rate is the average value at the equator at T_c.

Test #	$\Delta T/\Delta z$ (K m^{-1})	$\Delta T/\Delta t$ (K m^{-1})	B_a (μT)	B_{sc}/B_n	R_{res} (nΩ)	Δ/k_BT_c
1	22 ± 1	4.2 ± 0.6	0.21 ± 0.03	N/A[a]	9.9 ± 0.2	1.88 ± 0.01
2	0.3 ± 0.1	0.02 ± 0.01	0.2 ± 0.1	1.1	10.2 ± 0.2	1.85 ± 0.01
3	24 ± 1	2.8 ± 0.3	2.0 ± 0.1	1.06	17.5 ± 0.2	1.86 ± 0.02
4	0.2 ± 0.1	0.01 ± 0.01	2.0 ± 0.1	1.04	18.6 ± 0.2	1.85 ± 0.01
5	21 ± 1	10 ± 1	4.0 ± 0.1	1.02	26.9 ± 0.2	1.89 ± 0.01
6	0.5 ± 0.1	0.11 ± 0.01	4.0 ± 0.1	1.02	26.5 ± 0.2	1.85 ± 0.01
7	46 ± 1	1.1 ± 0.3	0.3 ± 0.1	1.1 ± 0.1	11.7 ± 0.3	1.84 ± 0.01

[a] The data show no sharp change of magnetic field at T_c (figure 2(a)).

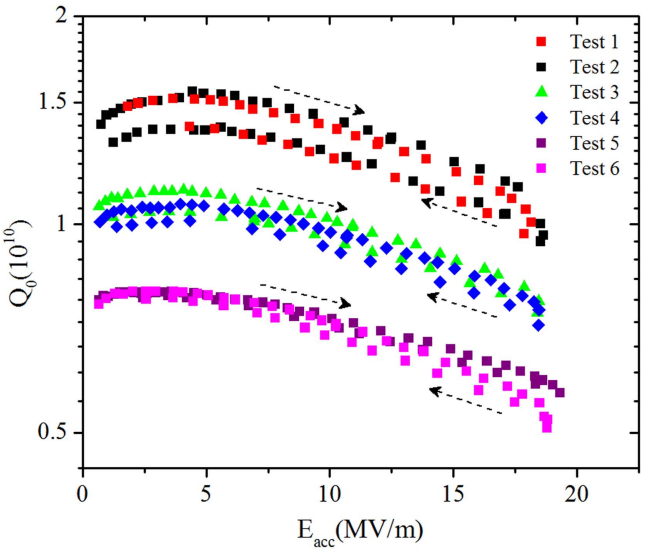

Figure 5. Q_0(2 K, E_{acc}) measured after each cooldown. All tests were limited by quench. The arrow represents the field increasing and decreasing direction after the cavity quench. Please refer to table 1 for the cooldown conditions for each test. The value of B_p/E_{acc} for this cavity shape is 4.21 mT (MV/m)$^{-1}$.

[11]. A warm-up above T_c and a subsequent cooldown would restore the initial Q_0-value.

To further explore the origin of the Q-degradation after quench, the cavity was disassembled, HPR, re-assembled and evacuated. Three Bartington single-axis cryogenic flux-gate magnetometers, labeled M1–M3, were placed along the equator, 120° apart, and directed along the cavity axis. Cernox temperature sensors were placed at ∼1 cm from each magnetometer and at the top and bottom iris. The cavity was cooled with a high temperature gradient (∼46 K m^{-1}) at T_c and the local residual magnetic field and temperature were monitored during the whole test, including the cooldown from room temperature to 1.6 K, the high-power rf test and warm up to 300 K. The local magnetic field measured at the three equator locations as the cavity crosses T_c is shown in figure 6: changes in amplitude, up to ∼0.5 μT, and direction of the magnetic field reflect the presence of thermo-currents driven by the non-uniform cavity temperature. As the cryostat filled with liquid He, changes in the permeability of the magnetic shield around the Dewar cause slow change in residual field at the cavity, up to ∼1 μT over ∼4 h. $Q_0(T)$ was measured from 4.3 to 1.6 K at low rf field ($B_p \sim 10$ mT). The $Q_0(E_{acc})$ was measured as part of the high-power rf test at 2 K and showed multipacting triggering multiple quenches at ∼15 MV m^{-1} (Test #7). The residual field measured by one of the magnetometers (M3) increased with each quench and showed some saturation at ∼3.0 μT, as shown in figures 6 and 7. Much smaller variations were measured by the other two sensors suggest that sensor M3 was somewhat close to the location where the quench occurred, although no temperature variation was measured by the sensor close to M3. This could be due to the high thermal conductivity of the Cu effectively dispersing the heat into the He bath and the exact location of the quench. The Q_0(2 K) at low rf field degraded by more than 50% after about ten quenches, as shown in figure 8. The data suggest trapping of additional residual field generated during each quench event and the saturation of trapped flux is consistent with earlier measurements reporting saturation of the surface resistance with extended quench events [11]. As the cavity is warmed-up, the magnetic field measured by sensor M3 drops abruptly as the temperature crosses above T_c, confirming that the additional field at sensor M3 resulted from trapped flux generated during quenches.

4. Discussion

Previous studies already showed that the performance of Nb/Cu clad cavities in terms of $Q_0(E_{acc})$ is comparable to that of bulk Nb cavities. In the last few years, several studies on the impact of cooldown and residual magnetic field on the residual resistance of bulk Nb cavities have been published and showed dependencies on grain size, surface treatment and orientations of both temperature gradients and residual field with respect to the cavity axis [15–24]. All these parameters influence the amplitude of the residual field, the fraction of residual field pinned in the Nb and the amplitude of the rf losses generated by the trapped flux. Whereas an earlier study suggested the cooling rate to be the main parameter determining the amount of flux pinned in the Nb [20], later studies showed that the temperature gradient along or across the

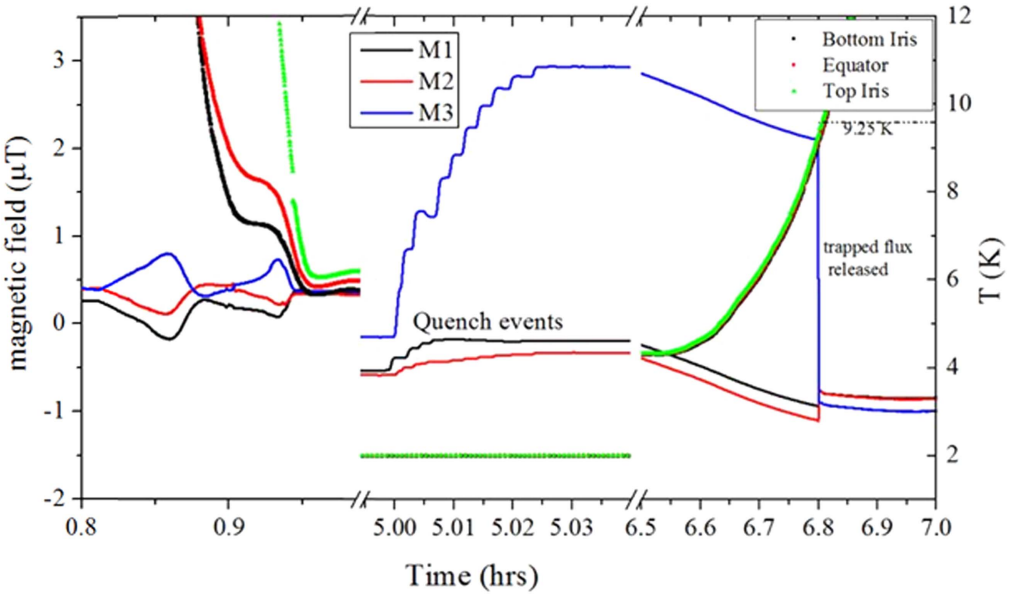

Figure 6. The magnetic field and temperature during cooldown, the high-power rf test and warm-up of cavity above 9.25 K.

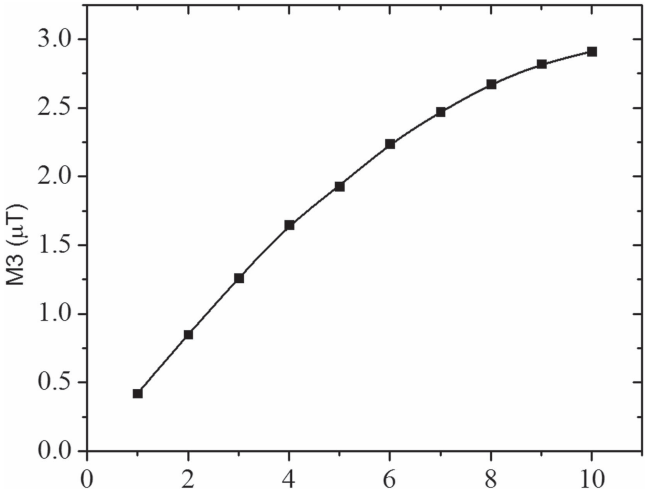

Figure 7. The amplitude of the magnetic field measured by sensor M3 during cavity quench events. The field saturated to ~3.0 μT after ten quenches.

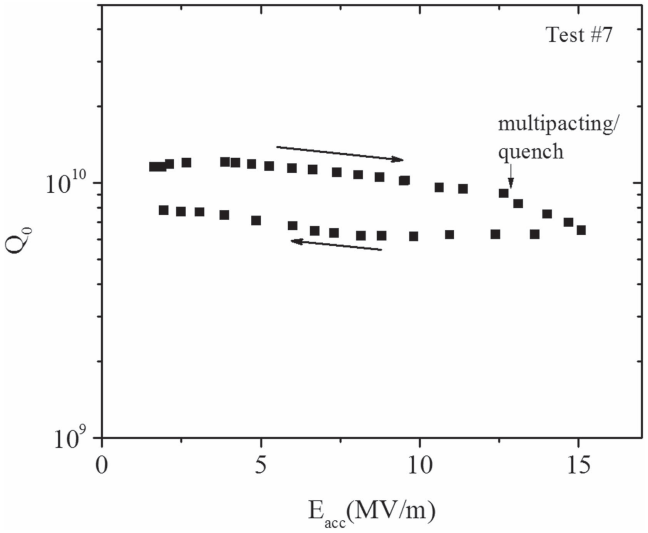

Figure 8. Q_0 (2 K, E_{acc}) measured during test#7 after cooldown with $\Delta T/\Delta z \sim 46$ K m^{-1} and an average residual field of 0.3 ± 0.1 μT at T_c, before and after multiple quenches induced by multipacting. The arrow represents the direction of increasing and decreasing rf field.

cavity axis is a key parameter [15, 18]. dR_{res}/dB_a measured in a fine-grain, electropolished bulk Nb cavity was 6 nΩ μT^{-1} [15] and the difference in R_{res} between 'fast' and 'slow' cooldown was ~1.5 nΩ [15]. Much higher values of $dR_{res}/dB_a \cong$ 30–40 nΩ μT^{-1} as well as larger increase of R_{res} for 'slow' cooldown compared to 'fast' cooldown were obtained for fine-grain, nitrogen-doped Nb cavities [17]. Values of dR_{res}/dB_a between ~0.6 and ~2.0 nΩ μT^{-1} were reported for a large-grain bulk Nb cavity treated by electropolishing (EP) and baking at 120 °C in ultra-high vacuum and cooled in temperature gradients ranging between ~1 and ~70 K m^{-1} [19]. Earlier measurements on a fine-grain Nb cavity reported dR_{res}/dB_a = 3.6 nΩ μT^{-1} [25].

Previous results on Nb/Cu clad cavities made by spinning showed more than one order of magnitude degradation of the quality factor for 'fast' cooldown (cooldown rate or temperature gradient values were not mentioned), compared to the Q_0 measured after thermal cycling at 10 K, and dR_{res}/dB_a = 5.6 nΩ μT^{-1} [26]. The value dR_{res}/dB_a =4.3 nΩ μT^{-1} obtained from our measurements on Nb/Cu cavity made by hydroforming and having a ~0.3 mm thick fine-grain Nb layer treated by EP is consistent with that of a regular ~3 mm thick Nb cavity with similar grain size and treatment. For temperature gradients up to ~46 K m^{-1}, the amplitude of the magnetic field generated by thermo-currents is ~0.3 μT which would correspond to changes in R_{res} of ~1 nΩ, of the same order as the experimental error in the measurement of R_s. The values of the ratio B_{sc}/B_{nc} in table 1 indicates that most of the residual field is trapped in the Nb.

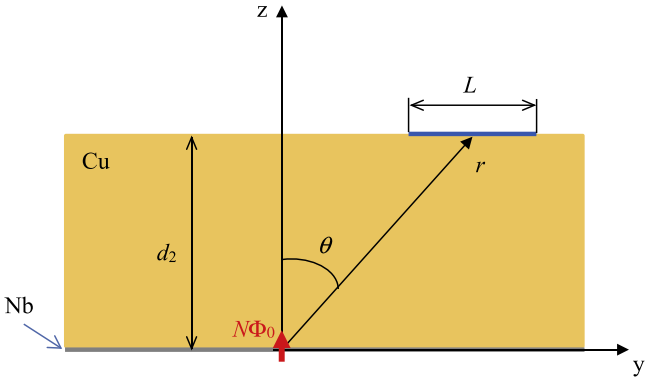

Figure 9. Schematic representation of the geometry used to estimate the number of trapped vortices after a quench based on the residual magnetic field measured by a single-axis magnetometer of length L.

In [12] it was speculated that the thickness of the Nb layer plays a role in determining the impact of thermoelectric currents and that thicker Nb (∼1 mm) would be preferred. A study on Nb/Cu cavities in which the Nb is a thin film, ∼1 μm thick, reported magnetic fields as high as 60 μT in the presence of a temperature gradient of ∼10 K m^{-1} [27]. The impact of such field on the residual resistance, however, is mitigated by dR_{res}/dB_a being about two orders of magnitude lower than in bulk Nb cavities. Recent work on another Nb/Cu thin film cavity showed a small reduction of R_{res} (less than 1 nΩ) when the cooldown rate was increased from 4.2 to 13.8 K min^{-1} and the corresponding temperature gradient increased by a factor of ∼7 [28].

Another type of bimetallic SRF cavity which has been investigated for many years is thin film (∼1.5 μm thick) Nb_3Sn grown on a ∼3 mm thick Nb substrate. A large, linear increase of the residual resistance with increasing temperature gradient along the cavity, of the order of 3 nΩ (K/m)$^{-1}$ was found for such cavities [29, 30]. A possible explanation could be related to the thermal conductivity of Nb_3Sn being about three orders of magnitude lower than that of Nb, therefore allowing much higher temperature non-uniformity, resulting in stronger thermo-currents.

A degradation of Q-values after quenching at high rf fields has been occasionally observed in bulk niobium cavities whereas and it has been commonly found in bimetallic cavities, both Nb/Cu and Nb_3Sn/Nb cavities [12, 27, 31]. It was found that the Q-value could be recovered by thermally cycling the bimetallic cavity above T_c, leading to the hypothesis of trapped flux due to thermo-currents created during quenches as the source of additional rf losses. In the case of bulk Nb cavities, a recent study showed no evidence of trapped flux induced by thermo-currents during quench events [32]. The data from the flux-gate magnetometers shown in figure 6 provide clear experimental evidence that such phenomenon occurs in a bimetallic cavity:

- additional magnetic field is generated during quenches and it is trapped in the Nb and
- the trapped flux is released as the cavity is warmed-up above T_c.

A possible explanation for the step-wise increase in the residual field after each quench event can be as follows: during the first quench a temperature gradient of the order of 20 K mm^{-1} (given that the thickness of the Nb layer is ∼0.3 mm and that the thermal conductivity of Cu is more than one order of magnitude greater than that of Nb) directed outward from the quench spot creates a thermo-current due to the Seeback effect, resulting in a magnetic field and a fraction of which is pinned in the Nb as the quenched region cools back below T_c. During the second quench, the thermal gradient is sufficiently strong to push vortices outside the extent of normal conducting region and get pinned there [33], while new vortices created by thermo-currents are pinned in the region close to the quench as it cools back down below T_c. This phenomenon, consisting in the accumulation of trapped flux at the edges of the quenched region and in the filling of that region with new vortices created by thermo-currents, as it becomes superconducting again, repeats with each quench event. Figure 7 shows that the amplitude of the residual field tends to saturate with increasing number of quenches, which might suggest a saturation of pinning centers. Some evidence for vortices pushed to and pinned at the edge of the normal conducting region during quench was given in [33].

In what follows we provide a quantitative estimate of the number of trapped vortices after each quench based on the magnetic field measured by magnetometer M3, which we expect to be in the vicinity of the quench spot given the high magnetic field value compared to that measured by M1 and M2. Referring to the schematic shown in figure 9, we approximate the bundle of N trapped vortices oriented normal to the Nb surface (z-direction in figure 9) as producing a magnetic flux $N\phi_0$ where ϕ_0 is the magnetic flux quantum. The single-axis magnetometer is a cylinder with an active region of length $L \cong 28$ mm, much larger than its radius (∼1 mm), oriented parallel to the surface at the equator (y-direction in figure 9) and at a z-position given by the thickness of the Cu layer, $d_2 = 2.5$ mm. Given that the distance between the magnetometer and the trapped flux is much smaller than the size of the cavity, the magnetic field generated by N vortices is given by [34]:

$$\vec{B} = \frac{N\phi_0}{2\pi r^2}\hat{r}. \tag{2}$$

The average field in the y-direction along the magnetometer whose center is at a distance r from the origin is given by

$$\langle B_y \rangle = \frac{1}{L}\int_{\theta_1}^{\theta_2} B_y\, r\, \mathrm{d}\theta = \frac{N\phi_0}{2\pi L\sqrt{d_2^2 + y_m^2}} \times (\cos\theta_1 - \cos\theta_2), \tag{3}$$

where $\theta_{1,2} = \cos^{-1}\left[1\Big/\sqrt{1 + \left(\frac{y_m}{d_2} \mp \frac{L}{2d_2}\right)^2}\right]$ and y_m is location of the center of the magnetometer on the y-axis. Assuming that the magnetometer was at a location for which $\langle B_y \rangle$ is maximum, $y_m = 14$ mm was determined numerically as the solution of $dB_y/dy_m = 0$. The amplitude of the field $\langle B_y \rangle$ measured by M3 after the first few quenches is ∼0.4 μT

and the number of trapped vortices which would produce such field, estimated from equation (3) is $N \cong 6 \times 10^5$.

The number of trapped vortices after recovering from each quench can also be estimated from the increase in the rf losses: the power dissipated in the cavity at $B_p \cong 10$ mT increased by ~28 mW after ten quenches. The power dissipated by a single vortex normal to the surface under a reasonable assumption that the mean length of the pinned vortex segment is greater than ~0.5 μm is given by [33]:

$$P_v = \pi H_p^2 \lambda \xi (\mu_0 \rho_n \omega / g)^{1/2}, \quad (4)$$

where λ is the rf penetration depth, ξ is the coherence length, ρ_n is the normal-state resistivity, ω is the rf angular frequency and g is related to the anisotropy of the superconductor. Taking $\lambda = 40$ nm, $\xi = 32$ nm, $\rho_n = 10^{-9}\ \Omega$ m and $g = 0.5$ for Nb and $H_p = (10\text{ mT})/\mu_0$, we obtain $P_v = 1.11$ nW. The average number of trapped vortices per quench can then be calculated by dividing 28 mW by P_v and the number of quenches resulting in $N \cong 2.5 \times 10^6$, which is in good agreement with the estimate based on the magnetometer data.

5. Conclusion

We have measured the effects of a temperature gradient and a residual magnetic field on the residual resistance of a Nb/Cu clad cavity. The results show that temperature gradients up to ~50 K m^{-1} have a negligible impact on the residual resistance. The sensitivity of the residual resistance to a residual magnetic field is similar to that of standard bulk Nb cavities with similar grain size and treatment. Multiple quenches lead to a higher residual resistance and the residual magnetic field measured by a flux-gate magnetometer clearly show that such increase is attributable to trapped flux. It is estimated that much higher temperature gradients than those applied during cooldown occur during quenches, resulting in stronger thermo-currents producing the magnetic field which can be trapped in the Nb layer. Estimates based on the additional residual magnetic field and rf losses suggest that a bundle of ~10^6 vortices are trapped in the Nb after a quench. It would be interesting to further investigate the impact of the thickness of the Nb layer as that affect the magnitude of the temperature gradient during quench and the distribution of pinned vortices close to the rf surface.

Acknowledgments

We would like to acknowledge W Singer from DESY for providing the NbCu clad cavity, P Kneisel (retired from Jefferson Lab), A Gurevich from Old Dominion University and S Calatroni from CERN for fruitful discussions. We would like to acknowledge Jefferson Lab technical staff for the cavity surface processing. This manuscript has been authored by Jefferson Science Associates, LLC under US DOE Contract No. DE-AC05-06OR23177.

ORCID iDs

Pashupati Dhakal https://orcid.org/0000-0002-9381-4091

References

[1] Valente-Feliciano A M 2016 *Supercond. Sci. Technol.* **29** 113002
[2] Benvenuti C *et al* 1999 *Physica* C **316** 153
[3] Cantacuzène S *et al* 1994 *Proc. EPAC* p 2076
[4] Fabbricatore P *et al* 1989 *J. Appl. Phys.* **66** 5944
[5] Müller Myers G S *et al* 1997 *Proc. 5th EPAC (Sitges Barcelona, 10–14 June 1996)* (Bristol: IOP Publishing) WEP002L 2085
[6] Posen S and Liepe M 2013 *Proc. 16th Int. Conf. on RF Superconductivity (Paris, France, September 2013)* TUP087 666
[7] Eremeev G *et al* 2013 *Proc. 16th Int. Conf. RF Superconductivity (Paris, France)* TUP071 603
[8] Oates D E, Agassi Y D and Moeckly B H 2010 *Supercond. Sci. Technol.* **23** 034011
[9] Gurevich A 2006 *Appl. Phys. Lett.* **88** 012511
[10] Fujino T *et al* 2000 *Proc. 3rd Superconducting Linear Accelerator Meeting in Japan (KEK Tsukuba, Japan, 25–26 May)*
[11] Singer W *et al* 2001 *Proc. 10th Int. Conf. RF Superconductivity (Tsukuba, Japan)* p PT006
[12] Saito K *et al* 2001 *Proc. 10th Int. Conf. RF Superconductivity (Tsukuba, Japan)* p 523
[13] Kneisel P and Ciovati G 2012 *JLab Technote* JLab-TN-12-033 JLab
[14] Halbritter J 1970 *External Report* 3/70-6 Karlsruhe Nuclear Research Center
[15] Romanenko A *et al* 2014 *J. Appl. Phys.* **115** 184903
[16] Gonnella D and Liepe M 2014 *Proc. 2014 Linear Accelerator Conf. (Lucerne, Switzerland)* p 84
[17] Gonnella A, Kaufman J and Liepe M 2016 *J. Appl. Phys.* **119** 073904
[18] Kubo T 2016 *Prog. Theor. Exp. Phys.* **6** 053G01
[19] Haung S, Kubo T and Geng R L 2016 *Phys. Rev. Accel. Beams* **19** 082001
[20] Vogt J-M, Kugeler O and Knobloch J 2013 *Phys. Rev. ST Accel. Beams* **16** 102002
[21] Gonnella D *et al* 2015 *J. Appl. Phys.* **117** 023908
[22] Martinello M *et al* 2015 *J. Appl. Phys.* **118** 044505
[23] Vogt J-M, Kugeler O and Knobloch J 2015 *Phys. Rev. ST Accel. Beams* **18** 042001
[24] Posen S *et al* 2016 *J. Appl. Phys.* **119** 213903
[25] Vallet C *et al* 1992 *Proc. EPAC'92 (Berlin)* p 1295
[26] Fujino T *et al* 1999 *Proc. SRF'99 (Santa Fe NM, USA)* p 372
[27] Calatroni S 2008 *J. Phys.: Conf. Ser.* **114** 012006
[28] Junginger T 2015 *Phys. Rev. Accel. Beams* **18** 072001
[29] Ciovati G, Eremeev G and Kneisel P 2012 *Jefferson Lab Technical Note* TN-12-021 Jefferson Lab
[30] Hall D L, Liarte D B, Liepe M and Sethna J P 2017 *Proc. IPAC'17 (Copenhagen, Denmark)* p 1127
[31] Knobloch J and Padamsee H 1997 *Proc. SRF'97 (Padova, Italy)* p 337
[32] Checchin M *et al* 2016 *Phys. Rev. Appl.* **5** 044019
[33] Gurevich A and Ciovati G 2013 *Phys. Rev.* B **87** 054502
[34] Kirtley J R 2010 *Rep. Prog. Phys.* **73** 126501